photonics

MDPI

Article

Single-Photon Transmission, Quantum Key Distribution, Multimode Fiber, and Higher-Order Poincaré Spheres

Daniel A. Nolan

Corning Inc., Corning, NY 14831, USA; nolanda@corning.com or danielnolan42@outlook.com

Abstract

In this study, we simulate the propagation of a single photon propagating within a modal group, traversing a multimode optical fiber in the presence of mode coupling. We illustrate the propagation graphically on a group of higher-order Poincaré spheres. The spheres display the propagation of the light within the modal group, including polarization in time and in distance as the transmission proceeds. Thus, the amplitudes and the relative phases within the group can be visualized throughout the transmission, which is novel and very useful for understanding the propagation. At the fiber output, we show how to recover the input of a classical state using the simulated propagation information displayed on such multiple spheres. Once a classical modal path is established from end to end, one can transmit quantum states, for example, as a spatial–time binned QKD (quantum key distribution) code. A quantum state follows this classical path. Hence, it can include binary or qudit information. Accessing a photon output state is important for many quantum network applications, including quantum key distribution, routing, and entanglement swapping. In addition, one can use other modal groups within the same fiber to multiplex other quantum channels as well as multiplex within a modal group using principal modes, a more complicated communication method. This situation is also discussed while considering the use of the spheres. Their applications include higher-dimensional quantum communications, quantum cryptography, and quantum networks. It is important to point out that in today's commercial quantum communications systems, quantum states are single-photon states, but they are not entangled. This includes both discrete and continuous variable quantum key distribution systems. Thus, in this report, we also address single-photon systems that are not entangled, unless stated otherwise.

Keywords: single photon transmission; multimode fiber; quantum key distribution; higher-order Poincaré sphere

Check for updates

Received: 18 July 2026
Revised: 23 August 2026
Accepted: 24 August 2026
Published: 31 August 2026

Copyright: © 2026 by the author. Licensee MDPI, Basel, Switzerland. This article is an open access article distributed under the terms and conditions of the Creative Commons Attribution (CC BY) license.

1. Introduction

Quantum communications and, in particular, quantum key distribution (QKD), are of significant worldwide interest. This is due to the increased interest in modular quantum computing [1] and in secure communications based on quantum physics [2–5]. Quantum technology is mostly based on the processing of qubits [6], referring to the quantum state that has a probability amplitude of being in one of two states, and qudits are quantum states that can be detected in one of 'd' states. There are advantages to processing quantum information with qudits rather than qubits, but the additional implementation complexity is often not well understood. This topic is now an important research subject for quantum information technology.

Within quantum communications, the transmission of quantum information using advanced states such as W and GHZ states [7,8] is of importance to current interests. A key advantage is that one can send more quantum information per photon and it enables more resilient quantum keys [9]. In this study, we investigate the possibility of transmitting 'd'-level quantum states through a multimode optical fiber, both in theory and via modeling. As an application, we consider transmitting a four-mode OAM (orbital angular momentum)–polarization quantum state through fiber in the presence of mode coupling. This is similar to transmitting a polarization-based qubit through a single-mode fiber in the presence of mode coupling, but is somewhat more complex. In the single-mode fiber case, one recovers the input polarization states using polarization controllers, by first establishing a path using classical light. Then, with the system link stabilized, the qubit can be transmitted and measured. The polarization controllers need to be monitored and adjusted using classical light in the order of minutes. In the OAM–polarization modal group case, a more complex quantum state results at the fiber output. Using the quantum field distribution, which we display on a group of higher-order quantum spheres, one can coherently combine both the spatial modal and polarization fields to recover the input state. One can then use quantum time binning to transfer quantum information. Today, time binning [10] is often used to transfer a quantum key through single-mode fiber links. In analogy to the BB84 protocol using linear or circular polarization for launching and detection, here, one uses an early or late time or, analogously to circular polarization, early–late time combinations with a phase relationship. Recently, 'd'-level time binning, including entanglement [11], has been demonstrated using a single-mode fiber.

The technology and photonic components required for the implementation of higher-dimensional quantum communications are currently being developed based on advancements in spatial-mode division multiplexing [12] for the purposes of increasing the capacity of classical optical communications by increasing the number of channels. Classical communications continue to grow at an exceptional rate. They are now being greatly enhanced by the communication demands resulting from rapid commercial hardware implementations of Artificial Intelligence (AI).

Interest is growing in commercial classical communications that use few-mode fiber and mode division multiplexing. Current commercial deployments incorporate MIMO [13,14] to handle the mode coupling that occurs during signal propagation. These systems require significant power to implement digital system processing and, therefore, are not suitable for quantum communications. Principal mode transmission, however, can be used to overcome the deleterious effects of mode coupling [15–18].

Apart from mode division multiplexing and principal mode transmission, higher-dimensional quantum communications are of interest in that one can transmit more information per photon [9] and in the advantages they offer to some quantum networks [19]. Thus, it is an objective of this communication to focus on the transmission of single photons through higher-dimensional space, but without the increased complexity of mode division multiplexing and principal modes. The coherent properties of the photon are important, as one needs to recover the input photon state to retain the quantum information or if one wants to implement entanglement swapping, which is of interest for long-distance communication [20] and quantum networks. For entanglement swapping, the photons being swapped need to be identical in polarization, spectrally, and in spatial mode. Otherwise, modal transformations are required before the swapping. In the single-mode fiber case, polarization controllers are used to regain the initial polarization state. This is required due to the polarization coupling that occurs during transmission. In the multimode, higher-dimensional situation, we require a similar method to regain the initial quantum state: the spatial–polarization mode. We investigate this by simulating the transmission of a single

photon through a four-transmission medium. With an end-to-end channel established, one can use time binning, including 'd'-level time binning, to transmit quantum information. We consider a two-polarization–two-spatial-mode system, such as an LP11 mode in an optical fiber. This numerical simulation is independent of the fiber index profile. The profile can be, for example, a step index or parabolic profile [21], but we are only concerned with the coupling within a modal group, such as the LP11 mode.

In Section 2, for modal propagation in an optical fiber, we write the mode coupling propagation equations for a photon transmitting through a four-mode (two spatial modes times two polarization modes) channel within a fiber. Such modes occur within the LPνμ mode of a multimode fiber [21]. In order to track and display the propagation, we propose using a group of higher-order Poincaré spheres [22,23]. Poincaré spheres are often used to display the polarization states of light propagating within a single-mode fiber as two polarizations propagate. Regarding higher-order modes, a higher-order Poincaré sphere has received much attention since its inception, and here, for the first time, we track the propagation along an input sphere and then the coupling to other spheres (adjacent modes) as the propagation progresses in the presence of mode coupling.

We can isolate the LPνμ mode in an optical fiber when the number of spatial–polarization modes is on the order of 16 modes, and the modal groups are on the order of 6 [24]. This is because the modes in an optical fiber separate into modal groups [21,25] that are nearly degenerate, and coupling between modal groups is minimal because the axial perturbations required to enable this coupling are on the order of millimeters, which is very unlikely. Coupling within a modal group is, however, likely because axial perturbations required to enable this coupling are on the order of meters or more, which is likely. A modal group typically includes two polarization modes and two spatial modes for $\nu > 0$, and two polarization modes and one spatial mode for $\nu = 0$. For this reason, we focus our attention on the propagation of a photon within a four-mode optical group.

Mode coupling in an optical fiber is a vast subject [25–32]. Gloge [27] showed that mode coupling among modes can be described with a diffusion equation. This is especially appropriate for fibers with many modes, because the simulation of power flow among these modes is of importance and the diffusion equation works well here. However, in many cases and in single-photon propagation, the amplitude and the phase of the propagating fields are important, and the power equations eliminate the phase information. In fact, the evolution of the phase values and the field amplitudes as the photon propagates within an optical modal group are key to understanding single-photon propagation in an optical fiber.

Here, we present a novel approach to the visualization of both the amplitude and the phase of a single photon as it propagates within an optical modal group of a multimode fiber. We display these values on multiple higher-order Poincare spheres. We limit the propagation of the light to within four LPνμ modes, and there is no coupling between the other modal groups. This sets the boundary to four modes, and coupling to other modal groups to zero, which is a very reasonable assumption.

In Section 3, we discuss how to use the calculated or experimentally determined classical field information to coherently combine the polarized–modal information to recover the input state. Once this is established, a time-bin quantum state can be transmitted and measured at the output. This recovery is necessary because any mode coupling distorts the coherence of the quantum state.

In Section 4, we discuss the relationship of the higher-order Poincaré sphere with the geometry of the quantum state and the implications of the SU(N) geometry and with principal modes.

In Section 5, we discuss and show the simultaneous propagation of multiple photon states.

In Section 6, we discuss the current research status as it relates to the implementation of higher-dimensional quantum communications.

2. Modal Propagation in Optical Fiber

The propagation of light in optical fiber is well described by the scalar wave equation [21], when the index difference between the core and cladding is on the order of a few percent. The axial solution is a propagating wave in z and is a function of the radius r, radial μ, and azimuthal ν, as well as the index distribution with the radius. The scalar wave equation is written as follows:

$$\frac{d^2F}{dr^2} + \frac{\frac{1}{r}dF}{dr} + \left(n^2k^2 - \frac{\nu^2}{r^2} - \beta^2\right)F = 0 \quad (1)$$

The scalar wave equation can be solved using the eigen solution method [21]. Here, a set of basis functions are used to obtain the wave functions, which are superpositions of these basis functions. Typically, Laguerre–Gauss functions are used as the basis functions, and the solutions are characterized as LP, linearly polarized modes. These solutions are functions of a radial function (μ) and an azimuthal function (ν). For ν not equal to 0, they are also characterized as orbital angular momentum modes. For circular cores, the LPνμ modes are separable in their radial, azimuthal, and axial components and can be written as follows:

$$\psi(\nu\mu) = A\mu\nu F\mu\nu(r)\exp(\pm i\nu\theta)\exp(-|i\,\beta z) \quad (2)$$

Spatial higher-dimensional quantum communications [9] intend to use these spatial distributions as channels for communication over distance.

As mentioned, in a multimode fiber, we can restrict single-photon propagation to within an LPνμ polarization–spatial mode. Since cross-coupling between LPνμ modes can be limited, we simulate the propagation of the single photon within the four modes of this polarization–spatial mode. In this manner, we obtain four modes, two polarization and two spatial. The +− signs represent alignment with the x and y axes.

Thus, we have four possibilities, and an unentangled W quantum state can be written as follows [7]:

$$W = 0.25^{0.5}\,[|-1,-1> + |1,-1> + |-1,1> + |1,1>] \quad (3)$$

In theory, one can use any LPνμ mode to transmit a W(4) state, but LP(ν = +−1, μ = 1, 2, 3) are most easily isolated in a fiber [21].

Mode coupling within these LP modes is common and expected due to stresses and strains on the fiber due to deployment. The mode coupling equations describing this coupling were described by Matera and Someda [33]. They described the polarization mode coupling in optical fiber. Consider now the propagation of the four modes within the LPνμ mode described above. Similarly to those of Matera and Someda, the mode coupling equations can be expressed as follows:

$$\frac{d\psi_i}{dz} = -i\beta\psi_i + \Sigma_j(-K_{ji}\,\psi_i + K_{ij}\,\psi_j) \quad (4a)$$

$$k_{ij} = j\,S \quad (4b)$$

These mode coupling equations are well known and used extensively to model the mode coupling properties of both spatial and polarization modes within a fiber. In Equation (4a), β is the propagation constant of the LP mode, and k denotes the mode coupling coefficients. In Equation (4b), S is a stress-optic coefficient [33]. These mode

coupling coefficients represent the effects of fiber twisting, bending, and core deformation, and these effects are well described by Ulrich and Simon [34]. In the simulation, we used their coupling coefficients for the case of twists, because twisting is the most effective way to implement mode coupling.

$$k = j\, n^2\, p_{44}\, \tau/2 \tag{5}$$

Here, τ is the twist rate per unit length, n is the core index, and p_{44} is one of the photoelastic coefficients, which is related to p_{11} (0.116 in silica) and p_{12} (-0.26 in silica) as follows:

$$p_{44} = (p_{11} - p_{12})/2 \tag{6}$$

Here, we use a twist rate of 2 twists per meter. It is important to note that these coupling parameters drift in time on the order of minutes depending on the fiber deployment and environment. Therefore, they can be considered constant for transmissions of hundreds of kilometers, and the system's transmission matrix can be fixed. However, the detection system needs to be capable of adjusting to this drift, and a new transmission matrix must exist, defined on this order in time. This is the situation in today's QKD systems, as the polarization controllers in the single-mode case are adjusted on this time scale.

To numerically solve Equations (4a) to (6), we used Python, version 3.11.4, as well as matplotlib.pyplot to plot the three-dimensional sphere information. The step size was set to 1. Using millimeters for the optical path length step size and lowering the step size to 0.1 mm did not affect the calculated propagation paths. The response length required to calculate the paths and display a sphere was less than a second. We chose a beat length of 1 and 0.5 m, but the calculations scale linearly with length. We chose these values because 1 m is typically selected to simulate polarization mode dispersion [34,35]. However, with today's commercial fibers, beat lengths are set to more than 10 times these values.

Light propagating and coupling between two polarizations in time can be displayed on a Poincaré sphere [23]. Born and Wolf show how to use the amplitudes and phase of the two components to plot the light's position on the sphere as the propagation continues:

$$S_1 = \left|E_1\right|^2 - \left|E_2\right|^2 \tag{7a}$$

$$S_2 = E_1\, E_2* + E_2\, E_1* \tag{7b}$$

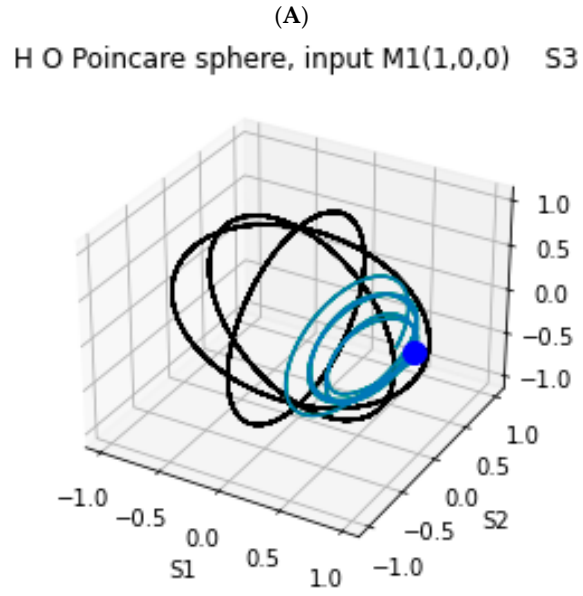
$$S_3 = \mathrm{j}(E_1\, E_2* - E_2\, E_1*) \tag{7c}$$

3. Mode Coupling, Mode Coherence, and Field Recombination at Fiber Output

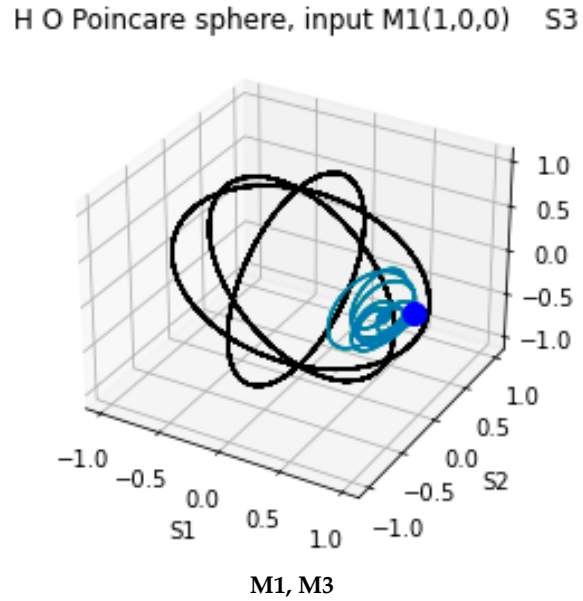
With four modes, there are six combinations of the fields of i and j. Thus, we can plot six spheres simultaneously as light propagates and then couples among the four modes. Then, for the four modes, we can take two modes at a time and plot a sphere for each, such that the spheres will be of (E1, E2; E1, E3; E1, E4), (E2, E3, E2, E4), and (E3, E4). If we input light into |1>|1>, the propagation combines mode |1,1> with |1,−1>. This is the combination of OAM1 and polarization +1, combining OAM1 with and polarization −1. The light propagates and couples with the parameters of Equations (4a) and (4b) under the coupling equations above, with a cross-coupling birefringence (beat length) of 1 m between the two OAM modes of two different polarizations and a beat length of one-half meter between an OAM mode of the same polarization. The beat lengths of the two polarizations in commercial optical fibers vary considerably, on the order of 1 to more than 10 m. In this simulation, we chose the meter lengths to be as mentioned above, but the results of the simulations scale with the transmission length vs. the beat lengths.

In this case, as the light from the input OAM mode of one polarization couples with the other polarization, the sphere has a radius of unity, but then, as the light begins to couple with the other possibilities, the radius of the tracked sphere shrinks, and the other sphere begins to appear and increase in radius. Below, we plot the six spheres as the light propagates up to 100 m. We used Python 3.11.4 3D graphics to plot the spheres, as shown in Figure 1A–C. At the output of the fiber, the light from each sphere can be coherently combined to a position on a defined sphere. Considering its applications, we discuss below how to combine these fields at the fiber output, enabling one to transfer a quantum state. In these figures, the black curves outline the surface of the sphere, and the green curve shows the trajectories of the light for the modes mentioned. The blue dot shows the position at which the light is input, always onto mode 1.

(**A**)

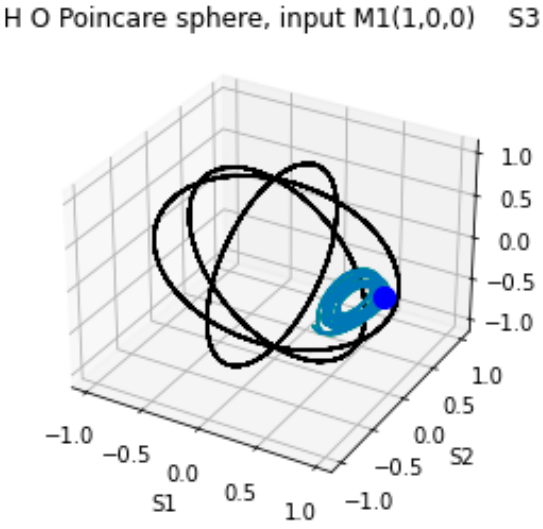


M1, M2



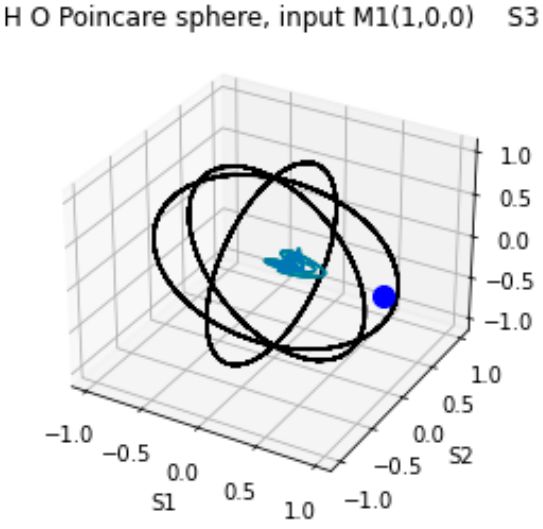
M1, M3

Figure 1. *Cont.*

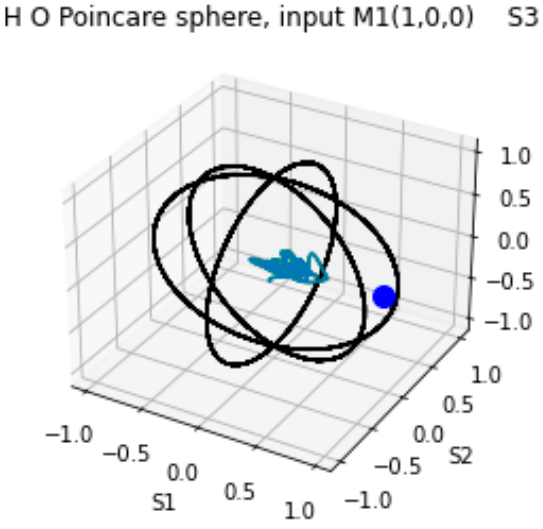


M1, M4

(**B**)



M2, M3
M2, M4



M2, M4

Figure 1. *Cont.*

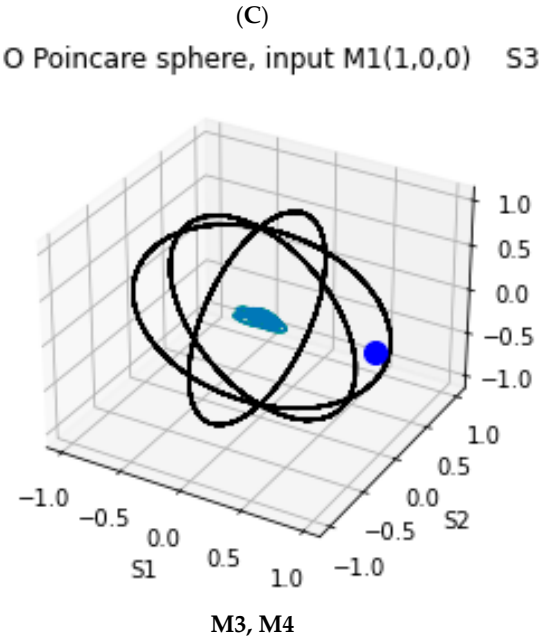


Figure 1. (**A**) HOM for modes 1 and 2, 1 and 3 and 1 and 4. Light is input onto mode 1, and the sphere position is indicated in blue. The coupling proceeds according to the green trajectory, and the sphere is outlined in black. (**B**) HOM for modes 2 and 3, and 2 and 4. Light is input onto mode 1, and the position is indicated in blue on the sphere. The trajectory proceeds according to the green line and the surface of the sphere is indicated in black. (**C**) HOM for modes 3 and 4. Light is input onto mode 1, and the position is indicated in blue on the sphere. The trajectory proceeds according to the green line, and the surface of the sphere is indicated in black.

Consider the first three spheres above: M1, M2; M1, M3; and M1, M4. These spheres display the phase difference between the two fields Mi and Mj, as well as their amplitudes. Using the spheres in Figure 1A, one can relate the modal fields in M2, M3, and M4 to those of M1. Thus, M1 can be chosen as the reference to which the other fields relate. By rotating the spatial fields at the output and/or the polarizations to align, one can coherently combine the fields by shifting one field with respect to the other by the phase difference. The phase difference is proportional to S3. The phase at the polar Z-axis maximum is $\pi/2$. Experimentally, these phase differences can be implemented with, for example, a Cailabs C multiple beam phase controller. Specifically, the polarizations can be rotated with a half-wave plate, and the fields can be rotated with flat optics [35,36].

For example, amplitude and phase corrections need to be on the order of minutes or more for polarization of two polarization modes [37,38]. There is not much data on the requirements for spatial mode correction, but it is reasonable to assume that these correction times will be similar. Calilab devices exhibit insertion losses in the order of 1 to 3 dB and fiber losses in a long-distance quantum link of 0.15 dB/km. Thus, in accounting for this loss, corrected quantum bits are received on the order of seconds [38].

4. Multiple Higher-Order Poincaré Spheres and the Geometry of the Quantum State

The W state of Equation 3 can be used to transfer a qudit, which has more information per photon than a qubit [9]. As mentioned, we can achieve this using an LPνμ mode in an optical fiber. Due to mode coupling during propagation, the photon in an initial OAM state and polarization state can have a probability amplitude of being in the other OAM mode and/or the other polarization, as shown in Figure 1. A sphere represents the relative amplitude and phase of two electric fields. In the typical Poincaré sphere, this is the relation

between two polarizations, but also, in a higher-order Poincaré sphere, this is characteristic of the orbital angular momentum modes [39]. In our case, we have spheres combining two fields of a propagating OAM mode, which can have field combinations of a spatial field with a polarization and another spatial field with a different polarization.

Therefore, the photon output has a probability amplitude of being in each of the four positions with a specific value. Again, in our situation, the four positions are composed of two polarizations and two spatial modes. In single-mode optical fiber, the quantum state can be graphically displayed on the Poincaré sphere. In higher-dimensional quantum communications, the quantum states need to be displayed on a higher-dimensional sphere, which is something we cannot achieve in a three-dimensional world. Thus, we propose using a group of spheres to display the quantum information. The Poincaré sphere is used to display fiber polarization—propagation information in single-mode fiber, and this is an SU(2) quantum geometry. Any two-dimensional quantum state can be displayed on this sphere. In addition, any quantum state in this situation can be mathematically described as a specific sum of the Pauli matrices, which represents the quantum geometry of these states. Likewise, the geometry of an N-dimensional quantum state is an SU(N) geometry [18], and any state in an SU(N) geometry can be mathematically represented as a specific sum of the generalized Gell Mann $N^2 - 1$ generators quantified with the generalized Gell Mann matrices. Interestingly, through the use of these generators, principal states can be determined, enabling the possibility of spatial division multiplexing in the presence of mode coupling [18,40–42]. This is also the case with single-mode fiber, with which one can perform polarization multiplexing without crosstalk using principal states based on polarization, determined using the Pauli spin matrices. These principal states are launched using a combination of polarization modes mathematically described with the Pauli spin matrices [42]. In the case of multimode fiber, mathematically, generalized Gell Mann matrices are used to generate the launch conditions. Again, this is because any quantum state in an N-dimensional geometry can be described mathematically using the generalized Gell Mann matrices, and then crosstalk-free states are the principal states, solved with an eigen value matrix. The Gell Mann matrices are important as they relate to determining principal modes, because all states in these systems can be described using these matrices. This is why the principal states can be determined using them.

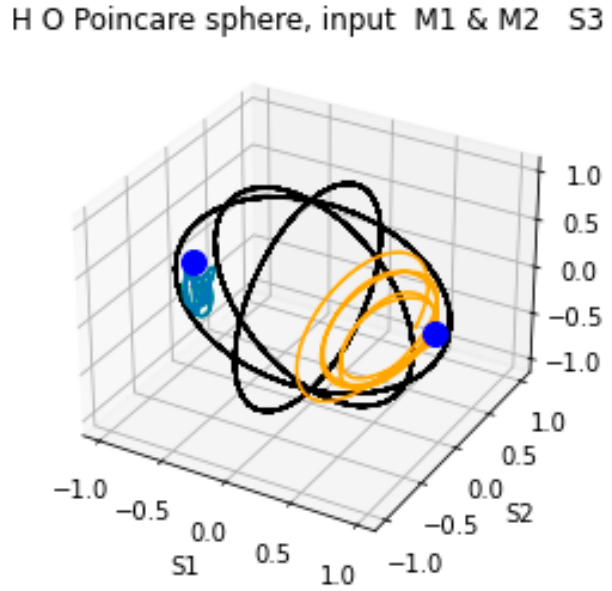
Most often, however, in today's commercial quantum communication QKD systems, multiplexing is not utilized, and principal states are not required. Because polarization mode coupling occurs during transmission, polarization controllers are required to coherently combine the transmitted state to the intended polarization state output.

5. Discussion: Multiple Photons

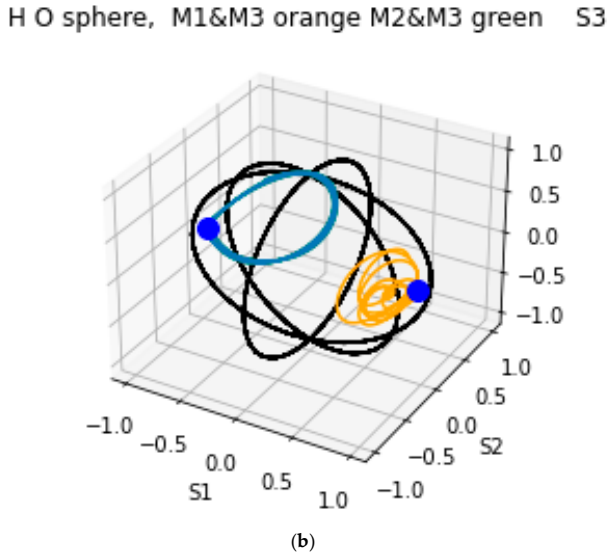
Regarding the geometry of the quantum state, we can also plot two separate input photons on the spheres. Figure 2 shows the trajectories of two photons on a sphere. One photon is launched onto mode 1, while a second photon is launched onto mode 2. The trajectories of photon 1, launched onto the fiber, oscillate more between modes 1 and 2 than those of photon 2. This is because photon 2 couples to mode 3 more easily than photon 1. This is because the difference in propagation constants between modes 1 and 3 is larger than that between modes 2 and 3. The differences between propagation constants significantly affect the amount of coupling [24]. The propagation constants for these simulations are chosen as below, with an index difference in each mode differing from the core index of 1.5. These index differences correspond to the beat lengths between the modes of a meter and one-half meter.

$$\beta_i = 2\ pi\ n_i/\lambda\ (\mathrm{i} = 1 \text{ to } 4) \tag{8a}$$

$$\begin{aligned} n_1 &= 1.5 + 0.0000015; \\ n_2 &= 1.5 + 0.00000075; \\ n_3 &= 1.5 - 0.0000007; \\ n_4 &= 1.5 - 0.0000015 \end{aligned} \tag{8b}$$



(**a**)



(**b**)

Figure 2. (**a**) Two photons are launched. Light is input onto mode 1, and the position is indicated in blue on the sphere. The trajectory proceeds according to the orange line. The modes considered are modes 1 and 2. Separately, light is launched onto mode 2, and the position is indicated in blue on the sphere. The trajectory proceeds according to the blue–green line. The surface of the sphere is indicated in black. (**b**) Two photons are launched. Light is input onto mode 1, and the position is indicated in blue on the sphere. The trajectory proceeds according to the orange line. The modes considered are modes 1 and 3, and the coupling is between modes 2 and 3. Separately, light is launched onto mode 2, and the position is indicated in blue on the sphere. The trajectory proceeds according to the green light. The surface of the sphere is indicated in black. In order to eliminate the interference of these 2 photons at a detector, one needs to use principal mode transmission as described above, since the presence of more than 1 single photon or channel leads us to multiplexing.

6. Outlook

Quantum communications is at an early stage of implementation. Applications are mostly in cryptography, such as in quantum key distribution using single-mode optical fiber and point-to-point systems. Higher-dimensional quantum communications are at early research stage. Their advantages include the possibility of quantum communication with more information per photon and multiplexing. Also, higher-dimensional quantum communications offer the possibility of new possibilities in network routing [19]. In addition, new, enhanced encryption methods and materials are being developed that can be applied here [36]. This is expected to be a very fruitful area of research and eventually lead to commercial applications. In network routing, routing is based on multiparticle entanglement, which can be based on wavelength, polarization, and spatial mode. In the long term, one can expect all three of these possibilities to be utilized. Regarding scalability, LP modes can be used to isolate uncoupled groups, and the modes in a selected LP mode can be used for transmission. For example, we can consider the LP modes in a ring core fiber [24,37]. The LP01 and LP02 modes can be used separately to transmit two polarization modes, and each of the LP11, LP21, LP31, LP12, and LP31 modes can be used to transmit four-mode quantum states. Quantum memories will also have a role to play, as memory will be used to store the photons for entanglement swapping. The number of wavelengths available in a quantum network will most likely be less than those in a classical network, due to the more complex requirements of these memories. Thus, additional entanglement parameters are required, such as space and polarization. It is also possible to include time as an entanglement parameter, but using time in this manner will slow down the network. Global research efforts regarding OAM hardware components, including OAM entanglement swapping [43–45], will continue. In fact, some of these components have been commercially available for more than 10 years, albeit at a low level.

Funding: This research received no external funding.

Data Availability Statement: The original contributions presented in this study are included in the article. Further inquiries can be directed to the corresponding author.

Conflicts of Interest: Author Daniel A. Nolan was employed by the company Corning Inc., Corning, NY 14831, USA. The author declares that the research was conducted in the absence of any commercial or financial relationships that could be construed as a potential conflict of interest.

References

1. Gent, E. The future of quantum computing is modular—Companies are thinking seriously about how to link quantum processors. *IEEE Spectrum* **2025**.
2. Bennett, C.H.; Broussard, G. Quantum Cryptography, Public key distribution and key tossing. In Proceedings of the IEEE International Conference on Computers, Systems and Signal Processing, Bangalore, India, 10–12 December 1984; pp. 175–179.
3. Korzh, B.; Lim, C.C.W.; Houlmann, R.; Gisin, N.; Li, M.J.; Nolan, D.; Sanguinetti, B.; Thew, R.; Zbinden, H. Provably secure and practical quantum key distribution over 307 km of optical fiber. *arXiv* **2014**, arXiv:1407.7427v1.
4. Lo, H.-K.; Curty, M.; Qi, B. Measurement-Device-Independent Quantum Key Distribution. *Phys. Rev. Lett.* **2012**, *108*, 130503. [CrossRef]
5. Boaron, A.; Boso, G.; Rusca, D.; Vulliez, C.; Autebert, C.; Caloz, M.; Perrenoud, M.; Gras, G.; Bussières, F.; Li, M.-J.; et al. Secure Quantum Key Distribution over 421 km of optical fiber. *Phys. Rev. Lett.* **2018**, *121*, 190502. [CrossRef]
6. Nielsen, M.; Chuang, I. *Quantum Computation and Quantum Information*; Cambridge University Press: Cambridge, UK, 2000.
7. Prevedal, R. *Experimental All-Optical One-Way Quantum Computing*; Sudwestdeutcher Verlag: Munich, Germany, 2009.
8. Cozzolino, D.; Da Lio, B.; Bacco, D.; Oxenløwe, L.K. High dimensional quantum communications: Benefits, progress, and future challenges. *Adv. Quantum Technol.* **2019**, *2*, 190038. [CrossRef]
9. Mirhosseini, M.; Magaña-Loaiza, O.S.; O'Sullivan, M.N.; Rodenburg, B.; Malik, M.; Lavery, M.P.J.; Padgett, M.J.; Gauthier, D.J.; Boyd, R.W. High-Dimensional Quantum Cryptography with Twisted Light. *New J. Phys.* **2015**, *17*, 033033. [CrossRef]

10. Boaron, A.; Korzh, B.; Houlmann, R.; Boso, G.; Rusca, D.; Gray, S.; Li, M.-J.; Nolan, D.; Martin, A.; Zbinden, H. Simple 2.5 GHz time–bin quantum key distribution. *Appl. Phys. Lett.* **2018**, *112*, 171108. [CrossRef]
11. Yu, H.; Sciara, S.; Chemnitz, M.; Montaut, N.; Crockett, B.; Fischer, B.; Helsten, R.; Wetzel, B.; Goebel, T.A.; Krämer, R.G.; et al. Quantum key distribution implemented with d-level time bin entangled photons. *Nat. Commun.* **2025**, *16*, 171. [CrossRef]
12. Richardson, D.; Fini, J.; Nelson, L. Space Division Multiplexing in Optical Fibers. *Nat. Photonics* **2013**, *7*, 354.
13. Van Uden, R.G.H.; Okonkwo, C.M.; Sleiffer, V.A.J.M.; de Waardt, H.; Koonen, A.M.J. MIMO equalization with adaptive step size for few mode fiber transmission systems. *Opt. Express* **2013**, *22*, 119–126. [CrossRef]
14. Karadimitrakis, A.; Debbah, M.; Moustakas, A. Optical MIMO: Results and analysis. In Proceedings of the IWCS 2014, Barcelona, Spain, 26–29 August 2014; pp. 966–970.
15. Fan, S.; Kahn, M. *Principal Modes in Multimode Fiber*; VDM Publications: Saarbrucken, Germany, 2010.
16. Carpenter, J.; Benjamin, J.; Eggleton, J. Comparison of principal modes and spatial eigenmodes in multimode fibre. *Lasers Photonics Rev.* **2016**, *11*, 1600259. [CrossRef]
17. Xiong, W.; Ambichl, P.; Bromberg, Y.; Redding, B.; Rotter, S.; Cao, H. Principal modes in multimode fibers: Exploring the crossover from weak to strong mode coupling. *arXiv* **2016**, arXiv:1609.025.
18. Milione, G.; Nolan, D.; Alfano, R. Determining principal nodes in multimode fiber, using mode delay method. *J. Opt. Soc. Am. B* **2015**, *32*, 143–149. [CrossRef]
19. Gu, X.; Chen, L.; Zeilinger, A.; Krenn, M. Quantum experiments and graphs III: High-dimensional and multi-particle entanglement. *arXiv* **2019**, arXiv:1812.095582v2.
20. Sangouard, N.; Simon, C.; de Riedmatten, H.; Gisin, N. Quantum repeaters based on atomic ensembles and linear optics. *arXiv* **2009**, arXiv:0906.2699v2.
21. Black, R.; Gagnon, L. *Optical Waveguide Modes*; McGraw Hill: New York, NY, USA, 2010.
22. Milione, M.; Szul, H.; Nolan, D.; Alfano, R. Higher order Poincare sphere and the angular momentum of light. *Phys. Rev. Lett.* **2011**, *107*, 053601. [CrossRef]
23. Born, M.; Wolf, E. *Principal of Optics*; Pergamon Press: Oxford, UK, 1959.
24. Ge, D.; Gao, Y.; Yang, Y.; Shen, L. A 6-LP-mode ultralow-modal-crosstalk double-ring-core FMF for weakly-couples MDM transmission. *Opt. Commun.* **2019**, *451*, 97–103. [CrossRef]
25. Marcuse, D. *Theory of Dielectric Optical Waveguides*; Academic Press: Cambridge, MA, USA, 1991.
26. Vassallo, C. *Optical Waveguide Concepts*; Elsevier: Amsterdam, The Netherlands, 1992.
27. Gloge, D. Optical power flow in multimode fibers. *Bell Syst. Tech. J.* **1973**, *51*, 1767–1783. [CrossRef]
28. Olshansky, R.; Nolan, D. Mode-dependent attenuation of optical fibers: Excess loss. *Appl. Opt.* **1976**, *15*, 1045–1047. [CrossRef]
29. Savovic, S.; Kovacevic, M.S.; Bajic, J.S.; Stupar, D.Z.; Djordjevich, A.; Zivanov, M.; Drljaca, B.; Simovic, A.; Oh, K. Temperature dependence of mode coupling in low-NA plastic optical fibers. *J. Light. Technol.* **2015**, *33*, 1. [CrossRef]
30. Birri, A.; McCary, K.; Wilson, B.A.; Blue, T.E. Thermally induced bend loss of optical fiber. *IEEE Sens. J.* **2018**, *18*, 6181–6187. [CrossRef]
31. Meunier, J.; Pigeon, J.; Massot, J. A general approach to the numerical determination of modal propagation constants and field distributions of optical fibers. *Opt. Quantum Electron.* **1981**, *13*, 71–83. [CrossRef]
32. Lavery, M.P.J.; Robertson, D.J.; Berkhout, G.C.G.; Love, G.D.; Padgett, M.J.; Courtial, J. Refractive elements for the measurements of the orbital angular momentum of a single photon. *Opt. Express* **2012**, *20*, 2110–2115. [CrossRef]
33. Matera, F.; Someda, C. Random birefringence and polarization dispersion in long single–mode optical fibers. In *Anisotropic and Nonlinear Optical Waveguides*; Elsevier: Amsterdam, The Netherlands, 1992.
34. Ulrich, R.; Simon, A. Polarization optics of twisted single-mode fiber. *Appl. Opt.* **1979**, *18*, 2241–2251. [CrossRef]
35. Li, M.; Nolan, D. Fiber spin profiles designs for producing fibers with low polarization mode dispersion. *Opt. Lett.* **1998**, *23*, 1659–1661. [CrossRef]
36. Yao, O.; Ma, Y.; Ma, C.; Zhang, H.; Huang, T.; Zheng, G.; Yu, S.; Li, Z. Flat optical rotator enabled by conformal mapping. *Laser Photonics Rev.* **2025**, *20*, e02470. [CrossRef]
37. Honjo, T.; Nam, S.W.; Takesue, H.; Zhang, Q. Long distance entanglement based quantum key distribution over optical fiber. *Opt. Express* **2008**, *16*, 19118–19126. [CrossRef]
38. Nadaalong, T. Automatic Compensation of Polarization Drift in an Optical Fiber. Bachelor's Thesis, Maximilians-Universitat, Munchen, Germany, 2018.
39. Berkhout, G.C.G.; Lavery, M.P.; Courtial, J.; Beijersbergen, M.W. Padgett, Efficient Sorting of Orbital Angular Momentum States of Light. *Phys. Res. Lett.* **2010**, *105*, 153601.
40. Nolan, D. Higher-Dimensional communications using multimode fibers and compact components to enable a set of communicating channels. *Optics* **2024**, *5*, 330–341. [CrossRef]
41. Nolan, D. Simulating Higher-Dimensional quantum communications using principal modes. *Optics* **2025**, *6*, 24. [CrossRef]

42. Gordon, J.; Kogelnik, H. PMD fundamentals: Polarization mode dispersion in optical fibers. *Proc. Natl. Acad. Sci. USA* **2000**, *97*, 4541–4550. [CrossRef]
43. Erhard, M.; Mehul, M.; Zeilinger, A. A quantum router for high-dimensional entanglement. *Quantum Sci. Technol.* **2017**, *2*, 014001. [CrossRef]
44. Lopez-Bastida, A.; Córdova-Morales, P.; Valdez-Pérez, D.; Martinez-Rivas, A.; de la Rosa-Vázquez, J.M.; Torres-Torres, C. Classical encryption demonstration with BB84 protocol–inspired coherent states using reduced graphene oxide. *Quantum Rep.* **2025**, *7*, 35. [CrossRef]
45. Graffitti, F.; D'AMbrosio, V.; Proietti, M.; Ho, J.; Piccirillo, B.; de Lisio, C.; Marrucci, L.; Fedrizzi, A. Hyperentanglement in structured quantum light. *Phys. Rev. Res.* **2020**, *2*, 043350. [CrossRef]

Disclaimer/Publisher's Note: The statements, opinions and data contained in all publications are solely those of the individual author(s) and contributor(s) and not of MDPI and/or the editor(s). MDPI and/or the editor(s) disclaim responsibility for any injury to people or property resulting from any ideas, methods, instructions or products referred to in the content.